Similar Solutions for the Hypersonic Laminar Boundary Layer Near a Plane of Symmetry

MASSIMO TRELLA* AND PAUL A. LIBBY†
Polytechnic Institute of Brooklyn, Freeport, N.Y.

The laminar hypersonic boundary layer near a plane of symmetry is treated from the similarity point of view. Cases of favorable and adverse pressure gradients in the plane of symmetry and of inflow to and outflow from that plane are considered. The similarity parameters are related to physical observables so that the results may apply, at least in terms of local similarity, to determine the boundary-layer characteristics in practical problems. It is found that crossflow has significant effects on the boundary layer in the plane of symmetry when the pressure gradient is adverse.

Nomenclature

A_i, B_i, C_i, $i = 1, 2, 3$ = integration const
C = ratio of $\rho\mu$ products, $\rho\mu/\rho_e\mu_e$
$c_f^{(x)}, c_f^{(y)}$ = skin-friction coefficients, cf. Eqs. (45)
f = transformed stream function for u velocity
F = y-wise shear function, cf. Eq. (53)
g = stagnation enthalpy ratio, $h_s/h_{s,e}$
G = x-wise shear function, cf. Eq. (50)
h = static enthalpy
h_s = stagnation enthalpy
j = index ($j = 0$ for flat surfaces, $j = 1$ for curved surfaces)
$\tilde{m}$ = external flow parameter, $\tilde{m} = u_e^2/2h_{s,e}$
m = exponent in x, $\bar{s}$ relation, cf. Eq. (21)
M_e = external stream Mach number
n = exponent in pressure distribution, cf. Eq. (29)
N_{St} = Stanton number, cf. Eq. (48)
p = static pressure
p_2 = curvature of pressure distribution in crossflow planes
q_w = heat transfer at the wall
r = radius of curvature of body in plane of symmetry, cf. Fig. 1
R = energy transfer function, cf Eq (55)
R_e^* = Reynolds number, $(2\bar{s})^{1/2}/\mu_e r^j$
$\bar{s}$ = similarity variable, cf. Eq. (4)
t = exponent in radius distribution, cf. Eq. (19)
u = velocity component in x direction
v = crossflow velocity gradient
$\mathbf{V}$ = velocity vector
x, y, z = boundary-layer coordinates, cf Fig 1
$\alpha, \hat{\alpha}$ = similarity parameter, cf. Eq. (23)
$\beta, \hat{\beta}$ = similarity parameter, cf. Eq. (15)
γ = ratio of specific heats
Γ = similarity parameter, cf. Eq. (24)
δ^* = displacement thickness
η = similarity variable, cf. Eq. (3)
θ = flow deflection from plane of symmetry
κ_1, κ_2 = constants in asymptotic solutions
μ = viscosity coefficient
ρ = mass density
$\tau_w^{(x)}, \tau_w^{(y)}$ = components of wall shear
φ = transformed stream function for crossflow

Subscripts

e = external flow
$k, k-1$ = iteration indices
0 = initial or reference conditions; conditions in plane of symmetry
1 = asymptotic solution

Received March 23, 1964; revision received July 27, 1964. This study was supported by the Air Force Office of Scientific Research Grant No. AF-AFOSR-62-409. The authors are pleased to acknowledge the capable assistance of Faiza Nabi in programing the numerical analysis.

* Research Assistant Professor of Aerospace Engineering; now on leave of absence. Member AIAA.

† Professor of Aerospace Engineering; now Professor of Aerospace Engineering, University of California at San Diego, La Jolla, Calif. Associate Fellow Member AIAA.

I. Introduction

THE characteristics of the laminar boundary layer in the neighborhood of a plane of symmetry are of interest in connection with a variety of high-speed flows. Perhaps the best known example thereof is the boundary layer on either the windward or the leeward side of a circular cone at an angle of attack. This example has been treated by Moore[1, 2] and Reshotko[3] for supersonic flow and recently by Cheng[4] for the hypersonic case.

More general examples of a boundary layer near a plane of symmetry arise on bodies of revolution at angles of attack and on lifting surfaces either with or without angles of attack. These flows involve pressure gradients in the plane of symmetry, either favorable or adverse, and a crossflow that may be either inflow toward or outflow from the plane of symmetry. The three-dimensionality in the preceding examples is due to the inviscid flow field associated with the surface geometry. There are, however, cases wherein interacting surfaces effectively uncouple the pressure distribution and surface geometry. An example is the boundary layer on a hypersonic inlet in the region of flow interaction between the cowling and the main body.‡ Finally, there may be mentioned flows involving three-dimensional pressure fields induced by the boundary-layer growth; such a flow would arise when either plates or wedges of finite span are placed in a low Reynolds number, high Mach number stream. If the span is sufficiently small so that the spanwise edges influence the boundary layer in the plane of symmetry, then an interacting boundary layer with either inflow or outflow from that plane would result.

In all of the foregoing examples prime interest concerns the influence of the crossflow on the gross boundary-layer properties such as boundary-layer thickness, skin friction, and heat transfer, and on the detailed profiles of the flow variables. Thus, e.g., there is suggested in Ref. 5 the possibility of employing outflow to reduce the boundary-layer thickness and either to prevent or to delay separation in the adverse pressure gradient of a hypersonic inlet.

In recent years it has been common in boundary-layer investigations to study cases wherein flow similarity prevails so

‡ Eli Reshotko, in a private communication, has called attention to another example of such a case, namely, the boundary layer on the side walls of two-dimensional wind-tunnel nozzles.

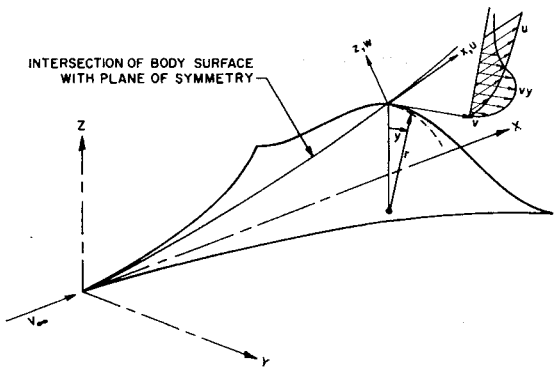

Fig. 1. Schematic representation of flow and coordinate system.[5]

that the entire boundary layer is characterized by solutions to a set of ordinary differential equations. With a pressure gradient in the plane of symmetry and curvature of the pressure field in cross planes, the similarity parameters applicable to two-dimensional or axisymmetric flows are supplemented by parameters related to the three-dimensionality. It is found[5] that only in the two limiting cases, either of low external Mach number ($M_e \sim \tilde{m} \simeq 0$) or of infinite external Mach number ($\tilde{m} \simeq 1$), is boundary-layer similarity possible. The former is a special case, i.e., specialized to a plane of symmetry, of the three-dimensional "cold-wall" flows treated by Vaglio-Laurin[6]; in these, the crossflow is such that the velocity vector within the boundary layer is almost coplanar with the velocity vector in the external flow and thus that there is little secondary flow.

The hypersonic limit requires mathematically an asymptotic treatment of the similarity parameters and of the stream function yielding the crossflow velocity profiles. The resultant analysis is thus strictly applicable only for $M_e \to \infty$ ($\tilde{m} = 1$) and leads to infinite overshoot for the crossflow velocity profiles. Thus, in contrast to the other limiting case, large skewing of the velocity vector within the boundary layer and large secondary flows occur with hypersonic Mach numbers in the external flow. The physical explanation of this behavior resides in the high gas density in the external flow relative to that within the boundary layer; thus, a three-dimensional pressure field leads to lateral motion of the gas within the boundary layer enormously greater than that in the external stream.

It is perhaps of interest to point out that solutions obtained from a consideration of the hypersonic limit may be applied for flows with finite but large Mach numbers external to the boundary layer according to the viscous hypersonic independence principle of Hayes and Probstein discussed in Refs. 7 and 8. It is to be expected on the basis of this principle that the boundary layer would be altered only in a thin layer near the outer edge as the Mach number in the external flow is changed from one large value to another. As pointed out in Ref. 5, such alterations could be computed by means of a systematic expansion of the nonsimilar equations in terms of a constant parameter $1 - \tilde{m}_0$ representative of external flow conditions; the zero-order solution is that of the hypersonic limit, whereas, it would be expected from the foregoing principle that the first-order corrections would be confined in the main to the outer portions of the boundary layer.

Because of the possible applicability of similar solutions for the laminar boundary layer near a plane of symmetry in the hypersonic limit, there are presented here solutions to the equations which are developed in Ref. 5 for such flows, but which are solved there only for the cases of small, i.e., linearized crossflow and of adverse pressure gradient in the plane of symmetry. Accordingly, there will be obtained here solutions for $\hat{\beta} \gtrless 0$ and $\hat{\alpha} \gtrless 0$, i.e., for favorable and adverse pressure gradients and for inflow and outflow. The gas will be assumed to be homogeneous, to have an approximate equation of state of the form $\rho \sim h^{-1}$, and to possess transport properties in accord with the frequently employed assumptions.

II. Analysis

The coordinate system and velocity components are shown in Fig. 1, which is taken from Ref. 5. The analysis proceeds by expanding the flow and geometric quantities in powers of the coordinate y as suggested by symmetry requirements. Introduction of these expansions into the boundary-layer equations for conservation of mass, of x-wise and y-wise momentum, and of energy, and consideration of only zero- and first-order terms in y leads to the set of partial differential equations describing the boundary layer near a plane of symmetry. The independent variables are x and z, and the dependent variables are the velocity components u and w, the mass density ρ, the stagnation enthalpy h_s, and the derivate with respect to y of the crossflow velocity denoted simply v. Thus the actual velocity either into ($v < 0$) or out of ($v > 0$) the plane of symmetry is vy whereas the crossflow "velocity profile" is given by v/v_e.§ The pressure field is characterized by $p(x,y) \simeq p_0(x) + y^2 p_2(x) + \ldots$ where, without ambiguity, the subscript zero may be dropped on p_0, and where p_2 is the curvature of the pressure in cross planes. The velocities in the external flow are related to the pressure field by

$$\rho_e u_e (u_e)_x = -(p_0)_x = -p_x \tag{1}$$

$$\rho_e u_e (r^j v_e)_x + \rho_e v_e^2 = -2p_2 \tag{2}$$

Similar solutions to these equations are now sought by introducing a two-component, i.e., vector stream function and new independent variables η, $\bar{s}$ after Levy-Lees where

$$\eta \equiv \rho_e u_e r^j (2\bar{s})^{-1/2} \int_0^z \frac{\rho}{\rho_e} dz' = \eta(x,z) \tag{3}$$

$$\bar{s} \equiv \int_0^x \rho_e \mu_e u_e r^{2j} dx' = \bar{s}(x) \tag{4}$$

The resulting ordinary differential equations with η as the dependent variable involve the usual similarity parameter for two-dimensional ($j = 0$) or axisymmetric flows, i.e., β, and two additional parameters α and Γ associated with the three-dimensionality.¶ Also explicitly appearing in these equations is the density ratio ρ_e/ρ; it is removed by introduction of the approximate equation of state $\rho \sim h^{-1}$ and by use of the definition of the stagnation enthalpy h_s. Finally, these equations contain a parameter which is associated with the Mach number of the external stream in the plane of symmetry, which is denoted $\tilde{m} \equiv u_e^2/2h_{s,e}$ and which plays an important role in establishing the possibilities for similar flow in the general case $\beta \neq 0$.

Final Equations and Their Physical Significance

Attention is now directed to the hypersonic limit $\tilde{m} \to 1$; in this case the similarity parameters β and α must approach zero while $\hat{\beta} \equiv \beta(1 - \tilde{m})^{-1}$, $\hat{\alpha} \equiv \alpha(1 - \tilde{m})^{-1}$ remain finite, and the function yielding the crossflow velocity profile must

§ Note that, for flat surfaces, the coordinate y is the Cartesian coordinate normal to the plane of symmetry, whereas for geometries with a radius of curvature r, the coordinate y is an angle as in Fig. 1. Thus the dimensions of v differ in the two cases, which are identified here by $j = 0, 1$ in the same manner as is customary in analyses treating simultaneously two-dimensional and axisymmetric flows.

¶ Note that Γ is denoted γ in Ref. 5. This change is made so as not to introduce ambiguity with respect to the ratio of specific heats in the external flow, a parameter involved in the present report but absent in Ref. 5.

be similarly stretched by $(1 - \tilde{m})^{-1}$. The resulting equations are

$$f''' + f''(f + \hat{\alpha}\varphi) + \hat{\beta}(g - f'^2) = 0 \tag{5}$$

$$\varphi''' + \varphi''(f + \hat{\alpha}\varphi) + \Gamma(g - f'^2 - \varphi' f') - \hat{\alpha}\varphi'^2 = 0 \tag{6}$$

$$g'' + g'(f + \hat{\alpha}\varphi) = 0 \tag{7}$$

where $(\ )'$ denotes differentiation with respect to η, and where, as is frequently done for simplicity, $C \equiv \rho\mu/\rho_e\mu_e$, and the Prandtl number has been taken to be unity. Equations (5–7) are to be considered the final equations being treated here; accordingly, it will be of interest to relate the dependent variables f, φ, and g and the similarity parameters to physically significant quantities.**

The quantities f and g have their usual physical significance

$$f' = u/u_e \qquad g \equiv h_s/h_{s,e} \tag{8}$$

so that the boundary conditions thereon are

$$\eta = 0 \qquad f' = 0 \qquad g = g_w = \text{const}$$
$$\eta \to \infty \qquad f' = g = 1 \tag{9}$$

The crossflow velocity profile is given by φ according to

$$\varphi' = v(1 - \tilde{m})/v_e \tag{10}$$

where in the hypersonic limit, $\tilde{m} \to 1$ and $v/v_e \gg 1$ within the boundary layer so that φ' is well defined. The velocity gradient v is more conveniently expressed as

$$v = [\hat{\alpha}\rho_e\mu_e u_e^2 r^{3j}/(2\bar{s})]\varphi' \tag{11}$$

which is well defined. Now the boundary conditions on φ' may be seen from Eq. (10); at the wall $v = 0$ and at infinity $v \to v_e$ so that when $\tilde{m} \to 1$ there are obtained

$$\eta = 0 \qquad \varphi' = 0$$
$$\eta \to \infty \qquad \varphi' = 1 - \tilde{m} \simeq 0 \tag{12}$$

The final boundary conditions on f and φ are imposed at $\eta = 0$; without loss of generality it is permissible[5] to take††

$$\eta = 0 \qquad f = \varphi = 0 \tag{13}$$

Similarity Parameters and Their Physical Significance

Consider next the similarity parameters, $\hat{\beta}$, $\hat{\alpha}$, and Γ. The first has its usual meaning in terms of $\bar{s}$, i.e.,

$$\hat{\beta} \equiv \{2\bar{s}/[u_e(1 - \tilde{m})]\}(du_e/d\bar{s}) \tag{14}$$

which may be written

$$\hat{\beta} = \bar{s}(1 - \tilde{m})^{-1}(d\tilde{m}/d\bar{s}) \tag{15}$$

so that

$$1 - \tilde{m} \sim \bar{s}^{-\hat{\beta}} \tag{16}$$

Now in the hypersonic limit $\tilde{m} \to 1$ it is understood that the proportionality factor in Eq. (16) is sufficiently small so that $\tilde{m} \simeq 1$.

The further discussion of $\hat{\beta}$ and the subsequent discussion of $\hat{\alpha}$ and Γ are facilitated if, as in Ref. 7, pp. 304–305, the gas in the external stream is considered to possess a constant ratio of specific heats γ. Then

$$h_e = h_{s,e}(1 - \tilde{m}) = [\gamma/(\gamma - 1)]p/\rho_e \sim p^{\gamma/(\gamma-1)} \tag{17}$$

so that Eqs. (16) and (17) yield

$$p \sim \bar{s}^{-\gamma\hat{\beta}/(\gamma-1)} \tag{18}$$

Furthermore, let

$$r \sim x^t \tag{19}$$

where clearly in the case of a flat surface $j = t = 0$, and take‡‡

$$\rho_e\mu_e \sim p \tag{20}$$

It is noted that the calculations carried out here have taken $t \geq 0$ but there can arise cases wherein $t < 0$ would prevail.

These assumptions, when applied in the hypersonic limit and when introduced into Eq. (4), result in

$$x \sim \bar{s}^m \tag{21}$$

where

$$m = \{[\gamma\hat{\beta}/(\gamma - 1)] + 1\}(2t + 1)^{-1} \tag{22}$$

Clearly then, Eqs. (19) and (21) imply that for conical bodies ($t = 1$) with $\hat{\beta} = 0$, $m = \frac{1}{3}$ as usual, and that, from a known pressure distribution $p = p(x)$ and a known value of t and γ, it is possible to determine the value of $\hat{\beta}$ for similarity.

With the geometry specified as by Eq. (19) the two parameters characterizing the crossflow are related as follows. By definition,

$$\hat{\alpha} \equiv [(2\bar{s})/\rho_e\mu_e u_e^2 r^{3j}][v_e/(1 - \tilde{m})] \tag{23}$$

$$\Gamma = (2\bar{s}/r^j v_e)[d(r^j v_e)/d\bar{s}] \tag{24}$$

Equation (24) implies

$$r^j v_e \sim \bar{s}^{\Gamma/2} \tag{25}$$

where again in the hypersonic limit, the proportionality factor is sufficiently small so that $v_e \simeq (1 - \tilde{m})$ as $\tilde{m} \to 1$. Now if $\hat{\alpha}$ is to remain constant, then the foregoing assumptions relative to the external stream and to the geometry, and Eq. (25) when considered in Eq. (23), lead to a relation

$$\Gamma = [8t/(2t + 1)] - 2 + [2\hat{\beta}/(\gamma - 1)] \times \{[4t\gamma/(2t + 1)] - 2\gamma + 1\} \tag{26}$$

which determines Γ once $\hat{\beta}$, t, and γ are selected. In the special case $\hat{\beta} = 0$, $t = 1$ corresponding to a cone, $\Gamma = \frac{2}{3}$ in accord with previous analyses thereof.[1–4]

The similarity parameter $\hat{\alpha}$ is related to physical quantities through Eq. (2); if therein, the derivative with respect to x is replaced by one with respect to $\bar{s}$, and if the definitions of $\hat{\alpha}$ and Γ are considered, Eq. (2) leads without approximation to

$$\Gamma + \hat{\alpha}(1 - \tilde{m}) = -2[p_2/(1 - \tilde{m})](2\bar{s}/\rho_e\mu_e u_e r^{2j})^2(\hat{\alpha}\rho_e u_e^2 r^{2j})^{-1} \tag{27}$$

In the hypersonic limit as $\tilde{m} \to 1$, and with the approximations attendant with the external flow and with the geometry, Eq. (27) leads to the requirement that

$$p_2 \sim \bar{s}^n \tag{28}$$

** It may be of interest to compare Eqs. (5–7) with $\hat{\beta} = 0$ to those of Cheng[4]; the independent variable $\eta = 2^{-1/2}\zeta$ and $f = 2^{-1/2}F$ where F and ζ are Cheng's variables; $\Gamma = \frac{2}{3}$; and $(1 - \tilde{m})^{-1}\alpha \equiv \hat{\alpha} = k$ in Cheng's notation.

†† Eli Reshotko has pointed out, in a private communication, that for the special case $\beta = 0$, $\Gamma = \frac{2}{3}$ a comparison of his solutions in Ref. 3 for $m < 1$ and of those of the present report for $\tilde{m} = 1$ leads to an indication of the practical applicability of the latter to cases $\tilde{m} \lesssim 1$. The indications are that $\tilde{m}$ must be greater than perhaps 0.98; it would thus appear that the series expansion scheme that is outlined in Ref. 5 and that permits systematic consideration of $1 - \tilde{m} > 0$ would be of practical interest.

‡‡ In Ref. 5 $\rho_e\mu_e$ was incorrectly taken to be constant so that the considerations leading to Eq. (27) therein are in error; accordingly, the linearized solutions presented there pertain to bodies whose distribution of radii r do not correspond to either bodies of revolution or flat surfaces as stated but rather to bodies with other power law variations of r.

where

$$n = 6mt - 2 - [3\gamma\hat{\beta}/(\gamma - 1)] \quad (29)$$

for similarity and to an equation yielding $\hat{\alpha}$ in terms of the physically measurable quantity p_2, namely,

$$\hat{\alpha} = -2[\gamma/(\gamma - 1)](\bar{s}/\rho_e\mu_e r^{3j})^2 (\Gamma h_{s,e})^{-1} (p_2/p) \quad (30)$$

From Eqs. (23) and (30) it may be seen that $v_e \sim -p_2\Gamma$ so that the occurrence of either inflow or outflow depends on the signs of both p_2 and Γ; e.g., if $\hat{\beta} = 0$ and $p_2 < 0$, $v_e > 0$ if $t > \frac{1}{2}$. This result indicates the coupling between the pressure field and the geometry.

It is perhaps appropriate to remark at this point that, as in all analyses based on similarity, the restrictions implied by Eqs. (18, 19, and 28) may apply in practical problems only over a range of x and/or $\bar{s}$; e.g., from Eq. (18) with $\hat{\beta} > 0$, $p \to \infty$ as $\bar{s} \to 0$. Thus it will be convenient as well as practical to assume below an initial length $x_0 > 0$ beyond which similarity prevails. When similar solutions are applied in this manner, there arises, of course, the question of how far downstream from x_0 the effect of the prior nonsimilarity persists. Such a question can only be answered by a nonsimilar, but perhaps linearized, analysis.

Transformed Streamwise Variable

In employing Eqs. (18, 28, and 30) for the selection of the appropriate values of the similarity parameters for a particular flow, it is necessary to have explicitly $\bar{s} = \bar{s}(x)$. Such a relation in accord with the assumptions relative to the external flow and to the geometry employed here can be developed as follows. Assume that there exists a length $x_0 > 0$ with a related $\bar{s}_0$ beyond which ($x > x_0$, $\bar{s} > \bar{s}_0$) similarity prevails. Assume further that at this station the quantities in the external flow are denoted by $(\ )_{e,0}$ and the radius by r_0^j. Then Eq. (4) leads to

$$\bar{s} - \bar{s}_0 = \rho_{e,0}\mu_{e,0}(2h_{s,e})^{1/2} r_0^{2j} x_0 m[(x/x_0)^{1/m} - 1] \quad (31)$$

which is the desired relation.

Asymptotic Solution

It is sometimes of interest in establishing uniqueness of solution and methods of numerical analysis of equations such as Eqs. (5–7) to consider the behavior of the solutions as $\eta \to \infty$. Accordingly, such solutions have been obtained here for Eqs. (5–7) following the methods employed in the past for two-dimensional and/or axisymmetric flows in, e.g., Ref. 9 and for three-dimensional flows in Ref. 10.

Let

$$\begin{aligned} f(\eta) &\simeq (\eta - \varkappa_1) + f_1(\eta) + \dots \\ \varphi(\eta) &\simeq \varkappa_2 + \varphi_1(\eta) + \dots \\ g(\eta) &\simeq 1 + g_1(\eta) + \dots \end{aligned} \quad (32)$$

where $\varkappa_1$ and $\varkappa_2$ are constants, where Eqs. (32) reflect the desired boundary conditions at $\eta \to \infty$, and where f_1, φ_1, and g_1 are considered the first-order deviations from infinity values and are required to vanish as $\eta \to \infty$. The equations for these deviations are obtained by substitution into Eqs. (5–7) and are conveniently written as

$$g_1'' + g_1'(\eta - \varkappa_1 + \hat{\alpha}\varkappa_2) = 0 \quad (33)$$

$$f_1''' + f_1''(\eta - \varkappa_1 + \hat{\alpha}\varkappa_2) - 2\beta f_1' = -\hat{\beta} g_1 \quad (34)$$

$$\varphi_1''' + \varphi_1''(\eta - \varkappa_1 + \alpha\varkappa_2) - \Gamma\varphi_1' = -\Gamma(g_1 - 2f_1') \quad (35)$$

so that g_1, f_1, and φ_1 can be solved for successively.

The solution for Eq. (33) with the appropriate condition at $\eta \to \infty$ is[9]

$$g_1 = -A_1(\gamma^{1/2}/2)\,\mathrm{erfc}[(\eta - \varkappa_1 + \hat{\alpha}\varkappa_2)/2^{1/2}] \simeq -(A_1/2^{1/2})(\eta - \varkappa_1 + \hat{\alpha}\varkappa_2)^{-1} \times \exp[-(\eta - \varkappa_1 + \hat{\alpha}\varkappa_2)^2/2] \quad (36)$$

where it is assumed that $(\eta - \varkappa_1 + \hat{\alpha}\varkappa_2)2^{-1/2} \gg 1$, and where A_1 is a constant of integration to be evaluated, e.g., from a numerical solution for g extended to sufficiently large η so that there apply the approximations attendant with Eqs. (32). Clearly, with one constant of integration, g can be made continuous at a matching point between the asymptotic solution with the correct behavior as $\eta \to \infty$ and a numerical solution, obtained by integration from $\eta = 0$; but a discontinuity in g' will in general occur there. Indeed the magnitude of the discontinuity in g' can be employed for the selection of the proper numerical solution, e.g., of the proper value of g_w'.

The solution for f_1' from Eq. (34) can be obtained in the usual manner from a linear combination of two complementary solutions and the particular solution; there results

$$f_1' = (\eta - \varkappa_1 + \hat{\alpha}\varkappa_2)^{-1} \exp[-(\eta - \varkappa_1 + \hat{\alpha}\varkappa)^2/2] \times \{B_1(\eta - \varkappa_1 + \hat{\alpha}\varkappa_2)^{-2\hat{\beta}} - (A_1/2)\} + B_2(\eta - \varkappa_1 + \hat{\alpha}\varkappa_2)^{2\hat{\beta}} \quad (37)$$

where B_1 and B_2 are constants of integration; a final integration of Eq. (37) would lead to a third integration constant B_3, which must be zero if $f_1 \to 0$ as $\eta \to \infty$. The constant B_2 is set equal to zero for all values of $\hat{\beta}$ according to the following reasoning; if $\hat{\beta} > 0$, B_2 must be zero to insure decay of f_1 as $\eta \to \infty$, whereas if $\beta < 0$, B_2 is set equal to zero to insure exponential decay of the boundary-layer solution into the solution for the external flow. It is this auxiliary condition that removes the nonuniqueness for such flows. The remaining constant of integration B_1 and the parameter $\varkappa_1$ may be selected so that the asymptotic solution is continuous in f and f' with a numerical solution extended to sufficiently large η so that Eqs. (32) apply. In this case the magnitude of the discontinuity in f'' at the matching point can be used as a criterion for the selection of a suitable numerical solution, e.g., of f_w''.

In a similar fashion, the solution for φ_1' can be obtained from two complementary solutions and a particular solution to Eq. (35). The analysis is simplified if B_2 is set equal to zero a priori; there results

$$\varphi_1' = (\eta - \varkappa_2)^{-1} \exp[-(\eta - \varkappa_1 + \hat{\alpha}\varkappa_2)^2/2]\{C_1(\eta - \varkappa_1 + \hat{\alpha}\varkappa_2)^{-\Gamma} - 2\Gamma B_1(\Gamma - 2\hat{\beta})^{-1}(\eta - \varkappa_1 + \alpha\varkappa_2)^{-2\hat{\beta}}\} + C_2(\eta - \varkappa_1 + \hat{\alpha}\varkappa_2)^{\Gamma} \quad (38)$$

where again, C_1 and C_2 are constants of integration, and where a third constant, which must be set equal to zero for $\varphi_1 \to 0$ as $\eta \to \infty$, will arise from a final integration. The previous discussion pertaining to the constants B_1 and B_2 in the equation for f_1 applies here as well; thus a numerical solution carried out to a sufficiently large η can be continued smoothly in φ and φ' to $\eta \to \infty$ through proper selection of $\varkappa_2$ and C_1;

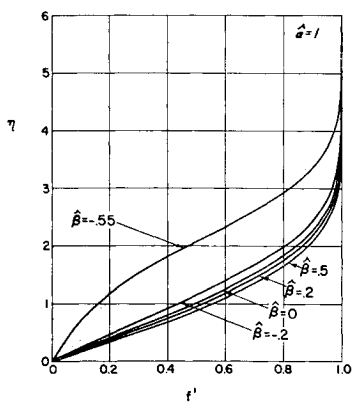

Fig. 2 Streamwise velocity profiles, $\hat{\alpha} = 1$.

the discontinuity in φ'' at the matching point can be used for the selection of the correct value of φ_w''. It is noted from Eq. (38) that, if $\Gamma - 2\hat{\beta} = 0$, then B_1 must be zero, and the solution for f_1' must be modified to include higher-order terms in the expansion for the complementary error function.

The main point of interest relative to the asymptotic solutions in the present report is the nonexistence of limitations on $\hat{\alpha}$, $\hat{\beta}$, and Γ imposed by the asymptotic behavior. This situation is in contrast to the case that pertains to the supersonic flow over a cone at an angle of attack ($\hat{\beta} = 0$, $\Gamma = \frac{2}{3}$, $\tilde{m} < 1$) and in which[1, 2] $\hat{\alpha} > -1$ in order for solutions to exist. This limitation is usually interpreted as a breakdown of flow similarity and not necessarily of the boundary-layer theory itself. It should be noted that this nonexistence of restrictions imposed by the asymptotic solutions does not guarantee the existence of numerical solutions for the whole range of η.

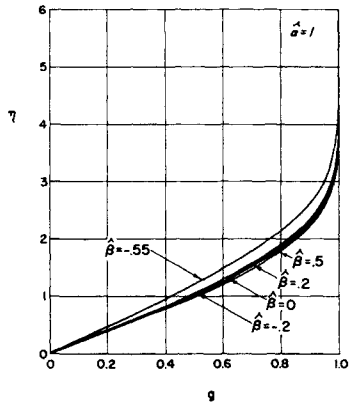

Fig. 3 Energy profiles, $\hat{\alpha} = 1$.

Three-Dimensional Displacement Thickness

There may arise in connection with the design of hypersonic inlets, and/or with the study of three-dimensional interaction effects describable by the present analysis, the need to compute the distribution of displacement thickness. Now it has been shown by Moore[1] and Lighthill[11] that the proper definition of displacement thickness, in the present case $\delta^* = \delta^*(x, y)$, is

$$\operatorname{div}\left[\rho_e \mathbf{V}_e \delta^* - \int_0^\infty (\varphi_e \mathbf{V} - \rho \mathbf{V}_e) dz\right] = 0 \tag{39}$$

For the coordinate system and flow considered here, and with

$$\delta^*(x, y) \simeq \delta_0^*(x) + y^2 \delta_2^*(x) + \ldots \tag{40}$$

Eq. (39) results to the lowest order in the equation

$$\left(\frac{d}{dx}\right)(\rho_e u_e \delta_0^*) = \frac{d}{dx}\left\{\rho_e u_e \int_0^\infty \left[1 - \frac{\rho u}{\rho_e u_e}\right] dz\right\} - r^{-j}\rho_e v_e \left\{\delta_0^* - \int_0^\infty \left[1 - \frac{\rho v}{\rho_e v_e}\right] dz\right\} \tag{41}$$

If now flow similarity prevails, and if the approximate equation of state $\rho \sim h^{-1}$ is applied, there results in the hypersonic limit $\tilde{m} \to 1$ to lowest order

$$\delta_0^* = \frac{(2\bar{s})^{1/2}}{\rho_e u_e r_0^j} (1 - \tilde{m})^{-1} \int_0^\infty (g - f'^2)\, dy \tag{42}$$

which leads, in accordance with the assumptions relative to the external flow and to the forementioned geometry, to

$$[\gamma p u_e / h_{s,e}(\gamma - 1)](2\bar{s})^{-1/2} r_0^j \delta_0^* = \int_0^\infty (g - f'^2)\, dy \equiv \Delta \tag{43}$$

The integral thickness Δ has been computed while obtaining the solutions presented here. It is noted that Δ appears explicitly in the method of solution of Eqs. (5–7), and that Δ is always finite provided asymptotic behavior involving exponential decay is required.

Skin Friction and Heat Transfer

Solutions to Eqs. (5–7) can be employed in the usual manner to compute the skin friction and heat transfer to the body. In the present three-dimensional flow, the wall shear has, of course, two components, which may be denoted $\tau_w^{(x)}$ and $\tau_w^{(y)}$, and which, in accord with symmetry requirements, may be expressed to lowest order as

$$\begin{aligned} \tau_w^{(x)} &\simeq \tau_{w,0}^{(x)} \\ \tau_w^{(y)} &\simeq y\tau_{w,1}^{(y)} \end{aligned} \tag{44}$$

Correspondingly, two skin-friction coefficients may be defined and expressed conveniently as

$$\begin{aligned} c_f^{(x)} &\equiv 2\tau_{w,0}^{(x)}/(\rho_e u_e^2) = 2f_w''(R_e^*)^{-1/2} \\ c_f^{(y)} &\equiv 2\tau_{w,1}^{(y)}\, y/(\rho_e u_e^2) = 2\hat{\alpha}\, \varphi_w''(\rho_e u_e r^j y/\mu_e)(R_e^*)^{-5/2} \end{aligned} \tag{45}$$

where $R_e^* \equiv (2\bar{s})^{1/2}/\mu_e r^j$. From Eqs. (45), the role of f_w'' and φ_w'' in the computation of the shear stresses is clear.

Note that the angle θ between the streamline at the surface ($z = 0$) and the plane of symmetry may be computed from $\tau_w^{(x)}$ and $\tau_w^{(y)}$; it is easy to show that

$$\tan\theta = (2\hat{\alpha}\varphi_w''/f_w'')(\rho_e u_e r^j y/\mu_e)(R_e^*)^{-2} \tag{46}$$

This angle should, of course, be compared to the corresponding angle that prevails in the external stream and that, in the limit as $\tilde{m} \to 1$, is zero.

The heat transfer to the surface is independent of y to first order, i.e., $q_w \simeq q_{w,0} + y^2 q_{w,2}$ so that

$$q_w \simeq q_{w,0} = \rho_e u_e h_{s,e}(R_e^*)^{-1/2} g_w' \tag{47}$$

and there can be defined conveniently a Stanton number

$$\begin{aligned} N_{St} &\equiv q_{w,0}/[\rho_e u_e h_{s,e}(1 - g_w)] \\ &= [g_w'/(1 - g_w)]R_e^{*-1/2} \end{aligned} \tag{48}$$

Method of Solution

Solutions of Eqs. (5–7) may be obtained by standard numerical methods for systems of ordinary differential equations. The only difficulty pertains to the two-point nature of the boundary conditions; for the equations of interest here numerical integration may be initiated at $\eta = 0$ provided values of f_w'', φ_w'', and g_w' are assumed and then successively corrected[10] such that, as $\eta \to \infty$, $f' = g = 1$, $\varphi' = 0$. However, it appears preferable to employ the iterative method, apparently due to Weyl[12] and used in Refs. 13 and 14 for simpler problems.§§

The details of the method are as follows. Let $G \equiv f''$ and write Eq. (5) in the iteration form

$$G_k' + G_k(f + \hat{\alpha}\varphi)_{k-1} = \hat{\beta}(f'^2 - g)_{k-1} \tag{49}$$

Equation (49) is interpreted as a first-order linear equation; the solution is

$$G_k = \exp\left[-\int_0^\eta (f + \hat{\alpha}\varphi)_{k-1} d\eta'\right]\left\{\hat{\beta}\int_0^\eta (f'^2 - g)_{k-1} \times \exp\left[\int_0^{\eta'} (f + \hat{\alpha}\varphi)_{k-1} d\eta''\right] d\eta' + G_{w,k}\right\} = f_k'' \tag{50}$$

§§ Note that other iterative methods of solution involving formal quadrature of the describing equation and integration by parts have been used in the past.[9, 15, 16]

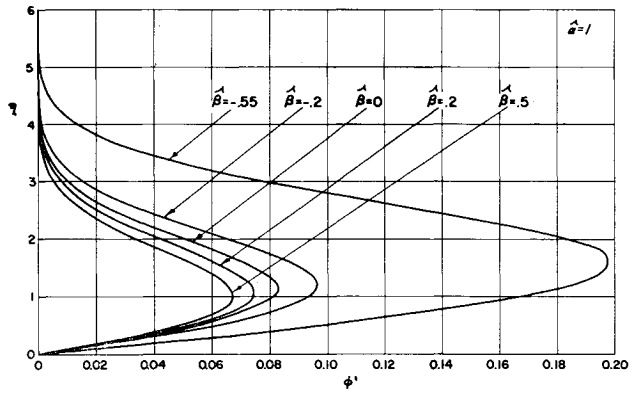

Fig. 4 Crossflow velocity profiles, $\hat{\alpha} = 1$.

where $G_{w,k}$ is the constant of integration. A second integration with $f_k'(0) = 0$ results in

$$f_k' = \int_0^\eta \exp\left[-\int_0^\eta (f + \hat{\alpha}\varphi)_k d\eta''\right]\left\{\hat{\beta}\int_0^\eta (f'^2 - g)_{k-1} \times \exp\left[\int_0^\eta (f + \hat{\alpha}\varphi)_{k-1} d\eta'''\right] d\eta'' + G_{w,k}\right\} d\eta' \quad (51)$$

Equation (51) applied at a large η with $f_k' = 1$ determines $G_{w,k}$. A final integration with $f_k(0) = 0$ may be written formally as

$$f_k = \int_0^\eta f_k' d\eta \quad (52)$$

Similar treatment is applied to Eqs. (6) and (7); thus let $F = \varphi''$, and $R \equiv g'$; there is obtained from Eq. (6) after two integrations

$$\varphi_k' = \int_0^\eta \exp\left[-\int_0^{\eta'} (f + \hat{\alpha}\varphi)_{k-1} d\eta''\right] \times \int_0^{\eta'}\left\{\hat{\alpha}\varphi_{k-1}'^2 - \Gamma(g - f'^2 - \varphi' f')_{k-1}\right\} \times \exp\left[\int_0^{\eta''} (f + \hat{\alpha}\varphi)_{k-1} d\eta'''\right] d\eta'' + F_{w,k}\Big\} d\eta' \quad (53)$$

Again if Eq. (53) is applied at a large η and φ_k' set equal to zero, then it is possible to evaluate $F_{w,k}$; a final integration with $\varphi_k(0) = 0$ yields

$$\varphi_k = \int_0^\eta \varphi_k' d\eta' \quad (54)$$

Similarly, two integrations of Eq. (7) result in

$$g_k - g_w = R_{w,k}\int_0^\eta \exp\left[-\int_0^{\eta'} (f + \hat{\alpha}g)_{k-1} d\eta''\right] d\eta' \quad (55)$$

where again $R_{w,k}$ is evaluated from Eq. (55) so that $g_k = 1$ for large η.

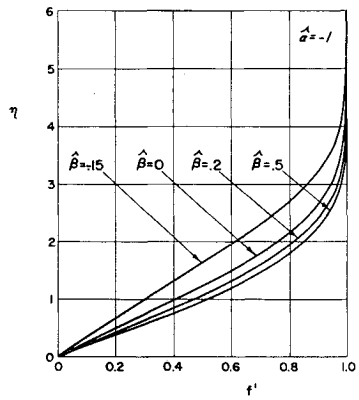

Fig. 5 Streamwise velocity profiles, $\hat{\alpha} = -1$.

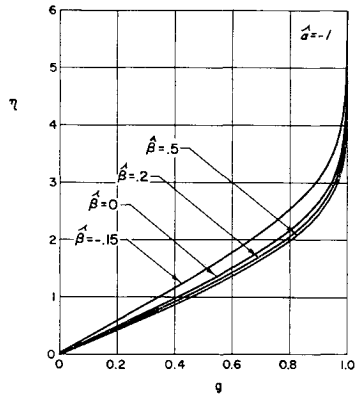

Fig. 6 Energy profiles, $\hat{\alpha} = -1$.

Remarks Concerning Numerical Analysis

A consideration of Eqs. (51–55) will show that a straightforward iteration procedure involving only quadrature can be carried out to find the functions f, φ, and g satisfying Eqs. (5–7), and the boundary conditions. Some remarks concerning the procedure as actually applied in the present report may be of interest. The quadratures were programed on a small scale computer, the RECOMP III, using a trapezoidal quadrature rule. The boundary conditions at "infinite" were generally imposed at $\eta = 6$; the values of f'', φ'', and g' obtained at this value after convergence to a solution were examined in each case and were found to be on the order of 10^{-7} or less.

For simplicity in programing, a uniform interval of η equal to 0.1 was used in the quadratures, although it was recognized that shorter computing time would have resulted if a coarse interval had been employed in the early iteration cycles, and a successively finer one, with interpolation employed, as a solution was approached.

The distributions required for initiation of iteration were taken to be f', φ', and g; Eqs. (52) and (54) were employed immediately to yield f and φ. These initial distributions were generally obtained from a solution corresponding to an "adjacent" solution in the following sense: It will be recognized that, if γ and t are selected, a solution is characterized by values of $\hat{\beta}$, $\hat{\alpha}$, and g_w, the value of the similarity parameter Γ being given by Eq. (26). It was the purpose of this study to examine the influence of these parameters on the boundary-layer properties so that a range thereof was covered. Thus a solution for one set of values was employed as the first approximation to the solution for a set in which one or more of the characterizing parameters were altered somewhat.¶¶

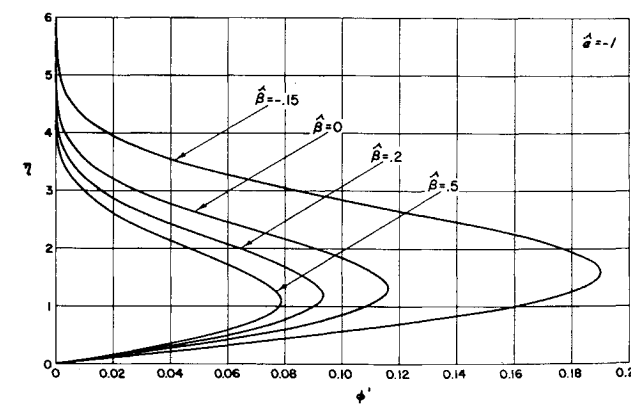

Fig. 7 Crossflow velocity profiles, $\hat{\alpha} = -1$.

¶¶ By obtaining the solutions in terms of f', φ', and g on tape as well as on conventional type-out, input handling was facilitated.

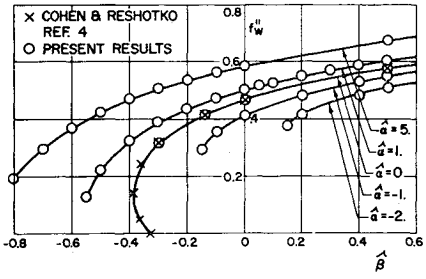

Fig. 8 Variation of streamwise wall-shear parameter.

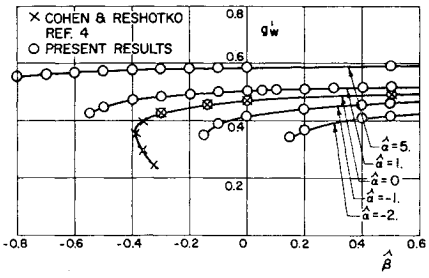

Fig. 9. Variation of heat-transfer parameter.

Convergence was monitored by examining successive values of the wall parameters f_w'', φ_w'', and g_w'; a solution was considered to have been obtained when $[(f_w'')_k - (f_w'')_{k-1}] \times (f_w'')_k^{-1}$, $[(\varphi_w'')_k - (\varphi_w'')_k^{-1}][(\varphi_w'')_k^{-1}$, $[(g_w')_k - (g_w')_{k-1}] \times (g_w')_k^{-1} \leq 10^{-4}$. In general convergence to these tolerances for $\hat{\beta}$, $\hat{\alpha} > 0$ was achieved in 3–4 cycles and required roughly 12–16 min. Rate of convergence degraded as either $\hat{\beta}$ or $\hat{\alpha}$ became negative, and indeed, as will be seen in "Discussion of Results," it was not possible with the direct iteration method described here to find solutions in some cases where, on the basis of existing results, e.g., for either $\hat{\beta} = 0$ (Ref. 4) or $\hat{\alpha} = 0$ (Ref. 9), solutions would be expected.

III. Discussion of Results

The values of the characterizing parameters for the solutions obtained in this study are displayed in Table 1. All solutions correspond to $\gamma = 1.4$, $g_w = 0$, which are perhaps the values of greatest practical importance; in addition most solutions correspond to $t = 1$, i.e., to bodies of conical shape, but additional solutions indicating the effects of variations in t have also been obtained. It is noted that the linearized results of Ref. 5 indicate some sensitivity of the boundary layer under consideration to the value of g_w, but additional solutions for various g_w, for $t < 0$, and for different γ are left for further study. Note of course that since γ and t appear only in Γ through Eq. (26) the present solutions may be employed for combinations thereof.

Table 1 Summary of numerical results; $\gamma = 1.4$, $g_w = 0$

$\hat{\alpha}$	$\hat{\beta}$	Γ	t	f_w''	g_w'	φ_w''
5	−0.8	0.4	1	0.1917	0.5533	0.1311
	−0.7	0.4333	...	0.2947	0.5640	0.1239
	−0.6	0.4667	...	0.3692	0.5706	0.1182
	−0.4	0.5333	...	0.4701	0.5784	0.1108
	−0.3	0.5667	...	0.5065	0.5810	0.1085
	−0.2	0.6	...	0.5372	0.5832	0.1067
	−0.1	0.6333	...	0.5635	0.5850	0.1054
	0	$\frac{2}{3}$	...	0.5867	0.5867	0.1045
3	0.5	0.8333	...	0.6426	0.5606	0.1065
2	0.5	0.8333	...	0.6249	0.5416	0.1088
1	−0.55	0.4833	...	0.1290	0.4257	0.1982
	−0.5	0.5	...	0.2228	0.4487	0.1749
	−0.4	0.5333	...	0.3271	0.4712	0.1518
	−0.3	0.5667	...	0.3914	0.4839	0.1388
	−0.2	0.6	...	0.4378	0.4925	0.1306
	0	$\frac{2}{3}$	...	0.5040	0.5040	0.1209
	0.1	0.7	...	0.5294	0.5083	0.1179
	0.2	0.7333	...	0.5515	0.5118	0.1157
	0.3	0.7667	...	0.5712	0.5149	0.1139
	0.4	0.8	...	0.5888	0.5177	0.1261
	0.5	0.8333	...	0.6048	0.5201	0.1115
−0.5	0	$\frac{2}{3}$	...	0.4478	0.4478	0.1354
−1	−0.15	0.6167	...	0.2951	0.3487	0.1923
	−0.1	0.6333	...	0.3595	0.3900	0.1631
	0	$\frac{2}{3}$	...	0.4175	0.4175	0.1447
	0.2	0.7333	...	0.4862	0.4433	0.1291
	0.4	0.8	...	0.5329	0.4578	0.1216
	0.5	0.8333	...	0.5520	0.4632	0.1193
−2	0.15	0.7167	...	0.3810	0.3432	0.1590
	0.2	0.7333	...	0.4164	0.3696	0.1474
	0.4	0.8	...	0.4875	0.4092	0.1301
	0.5	0.8333	...	0.5116	0.4199	0.1258
1	−0.2	−0.2	0	0.3441	0.4101	−0.07798
	...	0.4	0.5	0.4259	0.4818	0.09445
	...	0.6471	1.2	0.4402	0.4947	0.1385
	...	0.76	2	0.4456	0.4995	0.1566

The results are presented in terms of representative profiles of f', g, and φ' and of the variation with the similarity parameters $\hat{\beta}$, $\hat{\alpha}$, and Γ of the gross properties of the boundary layer such as the wall parameters, f_w'', g_w', and φ_w'', which are listed in Table 1 and which are displayed graphically as well.

Profiles

Figures 2–7 present the velocity and energy profiles for $\hat{\alpha} = 1, -1$, for various values of $\hat{\beta}$, and for $t = 1$. Consideration of Figs. 2 and 5 and of Figs. 3 and 6 indicates that the influence of inflow and outflow is relatively small on the f' and g distributions provided $\hat{\beta} \geq 0$, but that there is a strong effect of crossflow if $\hat{\beta} < 0$, i.e., if the pressure gradient is adverse. The crossflow profiles, on the contrary, are strongly dependent on the value of $\hat{\beta}$, whether it be either positive or negative.

Wall Parameters

Figures 8–10 show the variation with $\hat{\beta}$ and $\hat{\alpha}$ of the wall values f_w'', g_w', and φ_w'', respectively. Compared with Ref. 9 in Figs. 8 and 9 are the values of f_w'' and of g_w' for $\hat{\alpha} = 0$; similarly compared with Ref. 4 in Fig. 10 are the values of φ_w'' for $\hat{\beta} = 0$. The excellent agreement in all cases will be noted.

From Fig. 8 it will be noted that, for a given $\hat{\alpha}$, the effect of $\hat{\beta}$ on f_w'' appears qualitatively similar to that given for $\hat{\alpha} = 0$ in Ref. 9, i.e., there is a value of $\hat{\beta}$, below which no solutions exist and in the neighborhood of which there are two solutions. Unfortunately, as just implied, direct application of the iterative method of solution employed here permitted neither the quantitative determination of these minima nor

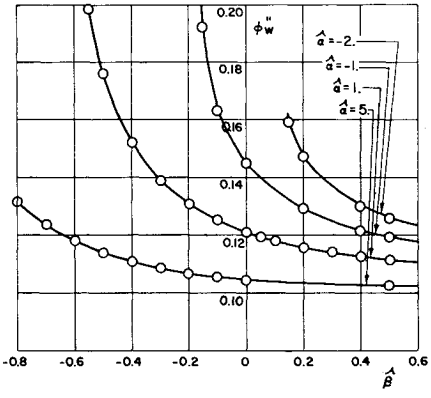

Fig. 10 Variation of crossflow shear parameter.

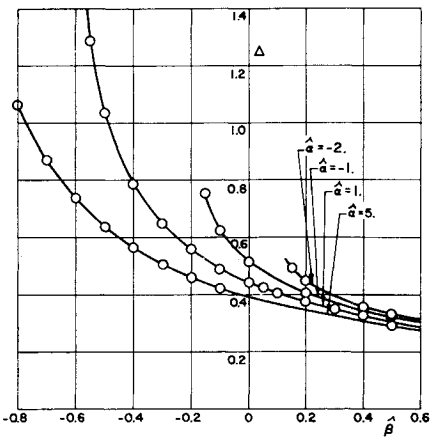

Fig. 11 Variation of displacement thickness integral.

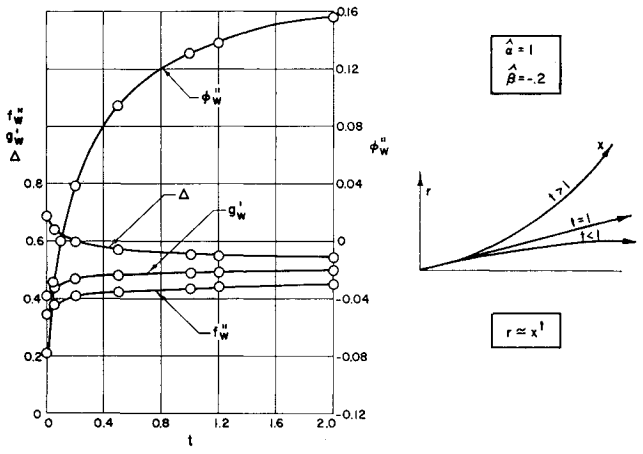

Fig. 13 Effect of geometry on flow parameters.

the demonstration of the multiple solutions for a given $\hat{\beta}$.* Also to be noted in Fig. 8 is the strong influence in delaying separation of outflow; this influence could only be indicated by the linearized analysis of Ref. 5.† The converse behavior of inflow is also shown in Fig. 8; indeed, it will be seen that for $\hat{\alpha} \lesssim -2$ no solutions exist unless $\hat{\beta} > 0$. The linearized analysis completely fails in these cases.

Figure 9 indicates relatively little effect of $\hat{\alpha}$ and $\hat{\beta}$ on the heat-transfer parameter g_w' except in the neighborhood of the minimum values of $\hat{\beta}$. There, large reductions in g_w' are seen to exist.

The effect of $\hat{\beta}$ and $\hat{\alpha}$ on the displacement thickness parameter Δ is shown in Fig. 11. Again it will be noted that significant alterations in this parameter occur when $\hat{\beta} < 0$, but that relatively small alterations arise when $\hat{\beta} > 0$. This result would seem to imply that relatively large values of $\hat{\alpha}$ are required if the interaction along a plane of symmetry of a finite-span plate is to be affected by spanwise flow. Whether such values of $\hat{\alpha}$ are realized cannot be estimated simply since they will depend on the geometry of the plate as well as the interaction itself.

In Fig. 12 there is shown a replot of the results of Fig. 8 to indicate the effect of $\hat{\alpha}$ on f_w'' for given values of $\hat{\beta}$, and to permit comparison with the results that are given in Ref. 4 and that pertain to $\hat{\beta} = 0$. The excellent agreement will be seen. It is noted from Fig. 12 that, for $\hat{\beta} < 0$, e.g., for $\hat{\beta} = -0.388$, the value of f_w'' is sensitive to small increments in $\hat{\alpha} > 0$. This implies that the linearized analysis of Ref. 5 can, in these cases, be applied only to a small range of $\hat{\alpha}$, whereas for $\hat{\beta} > 0$, a wider range of applicability prevails.‡

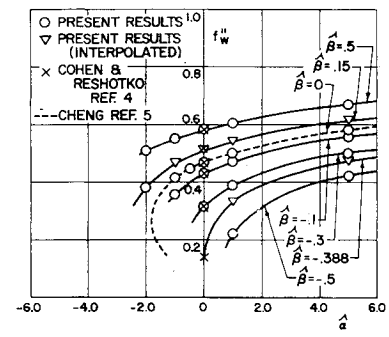

Fig. 12 Variation of streamwise wall-shear parameter.

The effect on the wall properties of geometry as contained in the parameter t ($r \sim x^t$) is shown in Fig. 13 for a pair of values $\hat{\alpha} = 1, \hat{\beta} = -0.2$. It will be appreciated from a consideration of Eq. (26) that the similarity parameter Γ changes as t changes. Indeed for $\gamma = 1.4$ and for this particular value of $\hat{\beta}$, $\Gamma = 0$ for $t = 0.1$; this implies from Eq. (30) that $p_2 < 0$ for $t < 0.1$. Of interest to note from Fig. 13 is that the solutions presented here for $t = 1$ appear to be applicable to a wide range of values of t provided $\Gamma > 0$.

Remarks Concerning Further Studies

It has been pointed out above that additional work can be done to obtain solutions for $g_w > 0$ and for $t < 0$, and that quantitative assessment of the duality of similar solutions in the neighborhood of the minimum $\hat{\beta}$ would also be desirable. It also may be noted that there might be some interest in the case of boundary layer near a plane of symmetry with mass transfer as, e.g., through a porous surface. The experiments in Ref. 17 indicate the importance of outflow and inflow on the normal forces arising on cones with mass transfer due to the lateral motion of the boundary layer from the windward to the leeward side, and to the alteration of the pressure distribution so as to reduce the normal force. This extension involves only making $f_w \neq 0$ in Eq. (13) but, of course, the mass-transfer rate per unit area per unit time must vary appropriately with x, i.e., as $(\bar{s})^{-1/2}$.

References

[1] Moore, F. K., "Three-dimensional boundary layer theory," *Advances in Applied Mechanics* (Academic Press Inc., New York, 1956), Vol. IV, pp. 160–224.

[2] Moore, F. K., "Laminar boundary layer on a circular cone in supersonic flow at a small angle of attack," NACA TN 2521 (October 1951).

[3] Reshotko, E., "Laminar boundary layer with heat transfer on a cone at angle of attack in a supersonic stream," NACA TN 4152 (December 1957).

[4] Cheng, H. K., "The shock layer concept and three-dimensional hypersonic boundary layers," Cornell Aeronautical Lab., Inc., Rept. AF-1285-A-3 (January 1961).

[5] Libby, P. A., Fox, H., Sanator, R. J., and DeCarlo, J., "Laminar boundary layer near the plane of symmetry of a hypersonic inlet," AIAA J. 1, 2732–2740 (1963).

* All methods of treating the two-point boundary conditions encounter difficulties in these cases. The present method may be altered so as to incorporate under or overrelaxation as in Ref. 9, but this was not done in the present study.

† In the numerical example of an axisymmetric body in a stream with $M_\infty = 20$, it is shown in Ref. 5 that values of $\hat{\alpha} \simeq 4$ can be obtained at an angle of attack as small as 2°; these data plus Fig. 8 imply significant alteration of separation characteristics due to outflow. They also indicate that values of $\hat{\alpha} > 5$, the maximum value considered here, may be of interest; indeed, Cheng carried out his calculation to $\hat{\alpha} = 15$.

‡ The linearized analysis yields essentially the slope $(df_w''/d\hat{\alpha})$ for $\hat{\alpha} = 0$, but a direct comparison between the present analysis and that of Ref. 5 is not possible in view of the different geometries considered here.

[6] Vaglio-Laurin, R., "Laminar heat transfer on three-dimensional blunt nosed bodies in hypersonic flow," ARS J. **29**, 123–129 (1959).

[7] Hayes, W. D. and Probstein, R. F., *Hypersonic Flow Theory* (Academic Press Inc., New York, 1959).

[8] Hayes, W. D. and Probstein, R. F., "Viscous hypersonic similitude," J. Aerospace Sci. **26**, 815–824 (1959).

[9] Cohen, C. B. and Reshotko, E., "Similar solutions for the compressible laminar boundary layer with heat transfer and pressure gradient," NACA TR 1293 (1956).

[10] Reshotko, E. and Beckwith, I., "Compressible laminar boundary layer over a yawed infinite cylinder with heat transfer and arbitrary Prandtl number," NACA TN 3986 (1957).

[11] Lighthill, M. J., "On displacement thickness," J. Fluid Mech. **4**, 383–392 (1958).

[12] Weyl, H., "On the differential equations of the simplest boundary layer problems," Ann. Math. **43**, 381–407 (1942).

[13] Bloom, M. H. and Steiger, M. H., "Perturbed boundary-layer solutions applied to the wall jet and Blasius profile," *Developments in Mechanics* (Plenum Press, Inc., New York, 1961), Vol. I.

[14] Janowitz, G. and Libby, P. A., "The effect of variable transport properties on a dissociated boundary layer with surface reaction," Polytechnic Institute of Brooklyn, PIBAL Rept. 804 (October 1963); also Int. J. Heat Mass Transfer (to be published).

[15] Hayday, A. A., "Mass transfer cooling in a laminar boundary layer in steady two-dimensional stagnation flow," Univ. of Minnesota, TN 19, Air Force Office of Scientific Research AFOSR TN 58-337, AD 154 241 (1958).

[16] Hoshizaki, H. and Smith, H. J., "The effect of helium injection at an axially symmetric stagnation point," J. Aerospace Sci. **26**, 399–400 (1959).

[17] Syvertson, C. A. and McDevitt, J. B., "Effects of mass addition on the stability of slender cones at hypersonic speeds," AIAA J. **1**, 939–940 (1963).

JANUARY 1965 AIAA JOURNAL VOL. 3, NO. 1

Magnus Characteristics of Finned and Nonfinned Projectiles

ANDERS S. PLATOU*
Ballistic Research Laboratories, Aberdeen Proving Ground, Md.

This is a summary of the Magnus force and moment measurements obtained on finned and nonfinned projectiles during the past several years. Most of the measurements have been obtained in the Ballistic Research Laboratories' (BRL) supersonic wind tunnels, with a few measurements taken in the BRL transonic range and the Naval Ordnance Laboratory's wind tunnels. The results have provided considerable insight into the generation of the Magnus force and moments on both finned and nonfinned projectiles. For nonfinned bodies at small angles of attack, having a laminar boundary layer, the Magnus force, at least on short bodies, obeys Martin's theory. At high angles of attack the Magnus force can be estimated from the lift force on a spinning cylinder flying perpendicular to the flow. The Magnus force on a spinning finned projectile is composed of two forces: a body force and a fin force. The forces normally act in opposite directions, thereby tending to cancel one another. However, the forces do not act at the same location; therefore a Magnus moment is created which is nearly independent of the center of gravity position. There are also two other known sources of Magnus moments on finned bodies which are created under certain conditions. These conditions are defined in this paper and the magnitude of the moments are estimated.

Nomenclature

a = speed of sound
b = fin span
d = major model diameter (also see Fig. 19)
r = radius of model or distance from center of rotation
c = fin chord
l = model length
M = Mach number $= U/a$
P_0 = stagnation pressure
P_b = fin base pressure
P_∞ = freestream static pressure
q = dynamic pressure $\frac{1}{2}\rho U^2 = \frac{1}{2}\gamma P_\infty M^2$
R_e = Reynolds number $\rho Ud/\mu$
R_l = Reynolds number $\rho Ul/\mu$
T_0 = stagnation temperature
t = fin thickness
U = freestream velocity
U_c = projectile cross velocity $U_c = U \sin\alpha$
S = body cross-sectional area $\pi d^2/4$
S_b = fin base area
A = body longitudinal cross-sectional area
y = radial distance from body centerline to fin cross section
α = angle of attack
α_B = body angle of attack
δ = fin angle of cant
ρ = freestream density
μ = freestream viscosity
ω = spin rate of model (plus is clockwise looking upstream)
ν = $\omega r/U$ or $\omega d/2U$
c.p. = Magnus force center of pressure from base
c.g. = center of gravity
C_L = lift force coefficient L/qS
C_N = normal force coefficient N/qS
$C_{N\alpha}$ = $dC_N/d\alpha$
C_m = pitching moment coefficient m/qSd
$C_{m\alpha}$ = $dC_m/d\alpha$
C_f = Magnus force coefficient $f/qS\nu$ (plus is to left looking upstream)
$C_{f\alpha}$ = $dC_f/d\alpha$
C_T = Magnus moment coefficient $T/qSd\nu$ (plus is plus force ahead of moment center)
$C_{T\alpha}$ = $dC_T/d\alpha$

Introduction

THE aerodynamic forces acting on a nonfinned body of revolution in free flight can only be influenced by spin through the viscous properties of the surrounding boundary

Received March 25, 1964; revision received June 12, 1964.
* Research Engineer, Supersonic Wind Tunnels. Member AIAA.